

Imprints of Primordial Non-Gaussianity on Gravitational Wave Spectrum

Caner Ünal

CEICO, Institute of Physics of the CAS, Na Slovance 2, 182 21 Prague, Czechia
School of Physics and Astronomy, University of Minnesota, Minneapolis, 55455, USA

Although Cosmic Microwave Background and Large Scale Structure probe the largest scales of our universe with ever increasing precision, our knowledge is still very limited for the smaller physical scales other than the bounds on Primordial Black Hole (PBH) amount. We show that the statistical properties of the small scale quantum fluctuations can be probed via the stochastic gravitational wave background, which is induced as the scalar modes re-enter the horizon. We found that even if scalar curvature fluctuations have a subdominant (or mild) non-Gaussian component, these non-Gaussian perturbations can source a dominant portion of the induced GWs. Moreover, the GWs sourced by non-Gaussian scalar fluctuations peaks at a higher frequency and this can result in distinctive observational signatures. If the induced GW background is detected, but not the signatures arising from the non-Gaussian component of the scalar fluctuations, $\zeta = \zeta_G + f_{\text{NL}} \zeta_G^2$, this translates into stringent bounds on f_{NL} depending on the amplitude of the GW signal.

I. INTRODUCTION

In the inflationary framework, the fluctuations at the largest scales of our observable universe are generated around 50-60 e-folds before the end of the inflationary era. The precise number depends on the details of the forthcoming stages which transfer the energy density from the inflaton to the light degrees of freedom. The large scale modes, with the corresponding wavenumbers $10^{-4} \text{Mpc}^{-1} \lesssim k \lesssim 0.1 \text{Mpc}^{-1}$, are probed by the Cosmic Microwave Background (CMB) and Large Scale Structure (LSS) experiments [1–3]. The spectral distortion experiments can further extend this range up to 10^4Mpc^{-1} [4–6]. However, even with these improvements, the scales that are probed with precision is only about 8 decades, or around 18 e-folds. Therefore, the remaining 30 – 40 e-folds of inflationary era in our horizon is mostly unexplored except the bounds on Primordial Black Holes (PBHs). This work aims at obtaining or constraining the physics at scales much smaller than the CMB by studying their imprints on stochastic gravitational waves (GWs).

Density and tensor fluctuations are generated and stretched to super-horizon scales during inflation. In later stages of the cosmic evolution, these modes re-enter the causal horizon eventually and lead to the current structure of our universe. In homogenous and isotropic backgrounds, at linear order, scalar, vector and tensor type fluctuations decouple, but starting from second order in perturbation theory, they interact with each other [7, 8]. We focus on GWs sourced by density perturbations that deviate from exact Gaussianity. We assume density perturbations with a dominant Gaussian (G) piece and a subdominant but nonvanishing local type non-Gaussian (NG) piece (except in Section II C, in which we discuss the case the scalar fluctuations are dominantly NG.).

We further assume an enhancement in scalar curvature power spectrum at scales that re-enter our horizon during radiation dominated era and much smaller than CMB scales. This enhancement can be a result of various reasons. One reason, for example, could be a feature in inflationary potential (a saddle point or a slope change)

[10–12]. Slowing down the inflaton might lead to significant quantum diffusion which influences the statistical properties of the scalar fluctuations [13–16]. Another reason could be the interaction of different fields and efficient particle production during inflation [17–19]. We do not assume any specific model, but a bump with non-vanishing local non-Gaussianity. We found that for a large range of density fluctuations, the resultant induced GWs are detectable at various current and future GW experiments.

The large density fluctuations leading to induced GW background can also produce abundant PBHs or compact massive objects [20, 21]. However, the PBH amount is extremely sensitive to the statistical properties of the density perturbations and threshold for the collapse. Therefore, the results of this work is expected to be valid independent of the fact that PBHs are a significant or a completely negligible fraction of the energy density.

II. GRAVITATIONAL WAVES INDUCED BY SCALAR PERTURBATIONS DURING RADIATION DOMINATION ERA

The second order tensor modes sourced by the first order scalar fluctuations have been studied long ago. We first give a brief summary of these results [7–9] and continue with the GW background from the non-Gaussian density fluctuations.

Ignoring vector, first order tensor perturbations and the anisotropic stress ([9] showed that its effect on GW spectrum is tiny.), we start with the following metric

$$ds^2 = a^2(\eta) \left[-(1 + 2\Phi) d\eta^2 + \left\{ (1 - 2\Phi) \delta_{ij} + h_{ij} \right\} dx^i dx^j \right]$$

where η is the conformal time, Φ the scalar gravitational potential and h_{ij} the second order tensor perturbation.

Fourier transformed tensor modes are expressed as

$$\hat{h}_{ij}(\eta, \mathbf{x}) = \int \frac{d^3\mathbf{k}}{(2\pi)^{3/2}} e^{i\mathbf{k}\cdot\mathbf{x}} \sum_{\lambda} \epsilon_{ij}^{\lambda}(\mathbf{k}) \hat{h}_{\lambda, \mathbf{k}}(\eta) \quad (1)$$

The equation of motion for the mode functions reads

$$h''_{\lambda, \mathbf{k}}(\eta) + 2\mathcal{H} h'_{\lambda, \mathbf{k}}(\eta) + \mathbf{k}^2 h_{\lambda, \mathbf{k}}(\eta) = 2\mathcal{S}_{\lambda, \mathbf{k}}(\eta) \quad (2)$$

where \mathcal{S} is the source term originating from first order scalar fluctuations (in the left panel of Fig. 1, this interaction, schematically $\zeta + \zeta \rightarrow h$, is shown).

$$\begin{aligned} \mathcal{S}_{\lambda, \mathbf{k}}(\eta) = & \int \frac{d^3 p}{(2\pi)^{3/2}} \epsilon_{ij}^\lambda(\mathbf{k}) p^i p^j \left[2\Phi_{\mathbf{p}}(\eta)\Phi_{\mathbf{k}-\mathbf{p}}(\eta) + \right. \\ & \left. + \left(\Phi_{\mathbf{p}}(\eta) + \frac{\Phi'_{\mathbf{p}}(\eta)}{\mathcal{H}(\eta)} \right) \left(\Phi_{\mathbf{k}-\mathbf{p}}(\eta) + \frac{\Phi'_{\mathbf{k}-\mathbf{p}}(\eta)}{\mathcal{H}(\eta)} \right) \right] \quad (3) \end{aligned}$$

where $\Phi_{\mathbf{k}}(\eta) = \frac{2}{3} T(k\eta) \zeta_{\mathbf{k}}$ and $'$ denotes $\frac{\partial}{\partial \eta}$. Here, $\zeta_{\mathbf{k}}$ is the scalar curvature fluctuation and T is the transfer function given as $T(x) = \frac{9}{x^2} \left[\frac{\sin(x/\sqrt{3})}{x/\sqrt{3}} - \cos(x/\sqrt{3}) \right]$.

The GW power spectrum is defined as usual

$$\langle \hat{h}_\lambda(\mathbf{k}, \eta) \hat{h}_{\lambda'}(\mathbf{k}', \eta) \rangle \equiv \frac{2\pi^2}{k^3} \delta^3(\mathbf{k} + \mathbf{k}') \delta_{\lambda\lambda'} P_\lambda(k), \quad (4)$$

Combining all these, we end up with

$$\begin{aligned} P_{h_i}(\eta, k) & \equiv \frac{k^3}{2\pi^2} \sum_{\lambda=\pm} \langle h_{i,\lambda}(\mathbf{k}) h_{i,\lambda}(\mathbf{k}') \rangle_\delta \\ & = \frac{64}{81} \frac{1}{2\pi^2} \frac{k}{\eta^2} \int \frac{d^3 p d^3 q}{(2\pi)^3} p^2 \sin^2 \theta_{\mathbf{k}\mathbf{p}} U(\mathbf{p}) q^2 \sin^2 \theta_{\mathbf{k}'\mathbf{q}} U(\mathbf{q}) \\ & \times \int_0^\eta d\eta' \int_0^\eta d\eta'' \eta' \eta'' \sin(k\eta - k\eta') \sin(k'\eta - k'\eta'') \\ & \times F_T(p\eta', |\mathbf{k} - \mathbf{p}| \eta') F_T(q\eta'', |\mathbf{k}' - \mathbf{q}| \eta'') \\ & \times \left\langle \hat{\zeta}_{\mathbf{p}} \hat{\zeta}_{\mathbf{k}-\mathbf{p}} \hat{\zeta}_{\mathbf{q}} \hat{\zeta}_{\mathbf{k}'-\mathbf{q}} \right\rangle', \quad (5) \end{aligned}$$

where $\cos \theta_{ab} = \hat{a} \cdot \hat{b}$ and $U(\mathbf{n}) = \cos(2\phi_{\mathbf{n}}) + \sin(2\phi_{\mathbf{n}})$. $\langle \rangle_\delta$ denotes correlation without $\delta^3(\mathbf{k} + \mathbf{k}')$. $F_T(u, v) = 2T(u)T(v) + \tilde{T}(u)\tilde{T}(v)$, where T is defined above and $\tilde{T}(x) = T(x) + xT'(x)$.

The current GW energy density (per logarithmic wavenumber) is linked with the GW power spectrum as

$$\Omega_{\text{GW}}(k, \eta_0) h^2 \simeq \frac{\Omega_{\gamma,0} h^2}{12} \frac{k^2}{a^2 H^2} \overline{\sum_\lambda P_\lambda}, \quad (6)$$

where the overbar indicates period averaging, $\Omega_{\gamma,0}$ is the current radiation density parameter.

We assume the scalar fluctuations which have the form

$$\zeta_{\mathbf{k}} = \zeta_{\mathbf{k}}^G + f_{\text{NL}} \int \frac{d^3 p}{(2\pi)^{3/2}} \zeta_{\mathbf{p}}^G \zeta_{\mathbf{k}-\mathbf{p}}^G \quad (7)$$

then ζ two-point function becomes

$$P_\zeta(k) = P_\zeta^G(k) + P_\zeta^{\text{NG}}(k) \quad (8)$$

and we parametrize the curvature fluctuations as

$$\begin{aligned} P_\zeta^G(k) & = \mathcal{A} \cdot \exp \left[-\frac{\ln^2(k/k_*)}{2\sigma^2} \right] \\ P_\zeta^{\text{NG}}(k) & = 2f_{\text{NL}}^2 \int \frac{dp d\Omega}{p 4\pi} \frac{k^3}{|\mathbf{k} - \mathbf{p}|^3} P_\zeta^G(p) P_\zeta^G(|\mathbf{k} - \mathbf{p}|), \quad (9) \end{aligned}$$

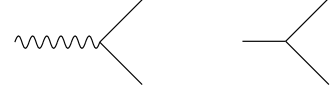


FIG. 1: Diagrammatic representation of $h\zeta\zeta$ and ζ^3 vertices

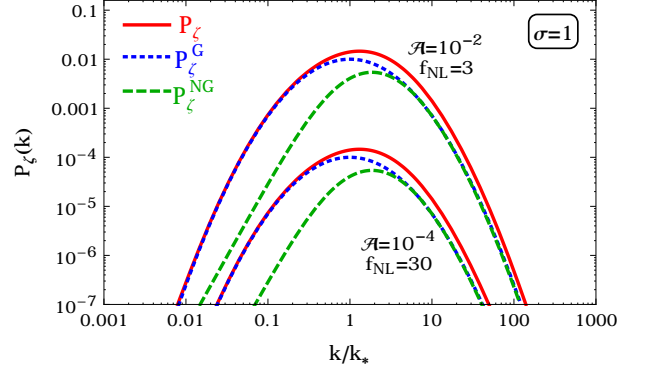


FIG. 2: Gaussian and Non-Gaussian components of P_ζ

where k_* is some comoving wavenumber that curvature perturbations have a bump at, \mathcal{A} is the amplitude at that scale and σ is the width of the signal in terms of e-folds. The vertex leading to local non-gaussianity is shown in the right panel in Figure 1). At CMB scales, curvature perturbations are nearly scale invariant and Gaussian, but on small scales the constraints are much weaker. We will focus on the case \mathcal{A} is much larger than the amplitude of the fluctuations at CMB/LSS scales and $\sigma \sim \mathcal{O}(1)$. Hence our findings will remain the same if one extends the CMB spectra via nearly scale invariant way.

Figure 2 shows the G and NG components of the scalar power spectrum. As a representative value, we choose $\mathcal{A} = 10^{-2}$, $\sigma = 1$ and $f_{\text{NL}} = 3$. By keeping $\mathcal{A} \cdot f_{\text{NL}}^2$ and σ constant, the relative amplitude of G and NG portions stay same (see also the case for $\mathcal{A} = 10^{-4}$, $\sigma = 1$ and $f_{\text{NL}} = 30$). Observe that in both cases, the NG spectrum is subdominant with respect to (or has similar amplitude with) G spectrum at every scale.

A. The Contribution of the Gaussian Source

When the scalar fluctuations are purely Gaussian, the GWs are sourced via the 1-loop diagram shown in Figure 3. A scale-invariant scalar power spectrum produces a scale-invariant GW energy density for the modes that re-enter the horizon during the radiation dominated era as $\Omega_{\text{GW}} h^2 \simeq 0.8 \Omega_{\gamma,0} h^2 \left(P_\zeta^G \right)^2$. For a bumpy scalar spectrum, the resultant GW energy density also becomes bumpy, and the peak of the GW is similar to the expression above with some $\mathcal{O}(1)$ correction depending on the width of the scalar signal.

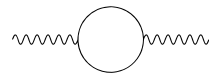


FIG. 3: Gaussian Sourcing of GWs

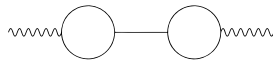


FIG. 4: Vanishing Non-Gaussian Source due to symmetry

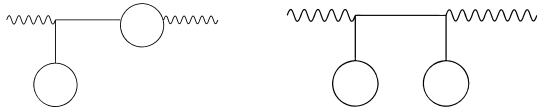


FIG. 5: Vanishing Non-Gaussian Source due to zero momentum scalar propagator

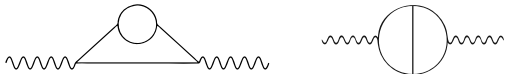
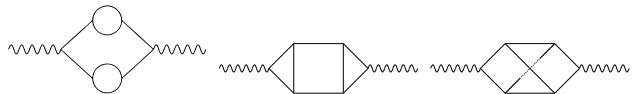
B. Contribution of the Non-Gaussian Sources

Non-Gaussian scalar fluctuations contribute to the induced GW background at f_{NL}^2 and f_{NL}^4 order via the 2 loop and 3 loop diagrams, respectively. There are 5 diagram topologies at f_{NL}^2 order, all shown in figures 4, 5 and 6. Some of these diagrams vanish and some of them contribute to the stochastic GW background. Moreover, there are more diagram topologies at f_{NL}^4 order, and we show only the non-vanishing ones in Figure 7. Here we discuss all the diagrams in detail.

Vanishing Diagrams with the Non-Gaussian Source: The three diagram topologies shown in Figures 4 and 5 do not contribute to the GW spectrum. The one in Figure 4 vanishes due to rotational invariance. The two diagrams in Figure 5 vanish since the tensor mode couples to scalar modes via derivative couplings. As the momentum of the propagator vanishes, this vertex does not contribute to the tensor two-point function. The same line of reasoning applies at $\mathcal{O}(f_{NL}^4)$ to the diagrams with zero-momentum scalar propagators at $h\zeta\zeta$ vertex.

Contributions at $\mathcal{O}(f_{NL}^2)$: There are two diagram topologies at f_{NL}^2 order that gives non-vanishing contribution to GWs. One diagram has both tree level and self-corrected scalar propagator, labeled as ‘‘Hybrid’’ (see the left panel of Figure 6). Since the loop correction to ζ can be factorized, this diagram can be reduced to two one loop calculations. The other diagram given on the right panel of Figure 6 is labeled as ‘‘Walnut’’ and is a non-reducible two-loop correction.

Contributions at $\mathcal{O}(f_{NL}^4)$: Neglecting the diagrams vanishing due to zero-momentum scalar propagators at $h\zeta\zeta$ vertex, we have three non-zero diagram topologies at f_{NL}^4 order given in Figure 7. The left diagram, labeled as ‘‘Reducible’’, can be expressed as three one loop diagrams (notice the two loops result from the scalar self correction). However, the other two diagrams are 3-loop diagrams which cannot be further factorized. We label these two diagrams as ‘‘Planar’’ and ‘‘Non-Planar’’ due to their topological properties. In this work, we only com-

FIG. 6: Diagrams contributing at f_{NL}^2 Order : Hybrid and WalnutFIG. 7: Diagrams contributing at f_{NL}^4 Order : Reducible, Planar, Non-Planar

pute Reducible diagram and estimate the contribution of the other two using earlier studies. These three topologies have been studied in [22] and it is found that Reducible and Planar diagrams have contributions within $\mathcal{O}(1)$ proximity and Non-Planar one is suppressed with respect to these two. Hence, in the rest of this work, we will take the total contributions from $\mathcal{O}(f_{NL}^4)$ diagrams as twice the contribution of the Reducible diagram.

C. Large ‘‘ f_{NL} ’’ (χ^2) Limit

In the limit of $f_{NL}^2 \mathcal{A} \gg 1$ (we stress that the expression in eq. (7) is not considered as a perturbative series expansion in orders of f_{NL}), we can absorb the f_{NL} parameter into definition of ζ_G such that $\zeta \simeq \pm(\zeta_G^2 - \langle \zeta_G^2 \rangle)$; hence the density fluctuations obey the χ^2 statistics. The relevant diagrams in that case are given in Figure 7. The PBH production and induced GW spectrum from χ^2 statistics have been studied for bumpy scalar fluctuations in [22]. (See [23, 24] for a detailed discussion of the effects of non-Gaussianity on PBH production, also [25], and [26] for an estimate of the resultant GW background.)

The induced GW background is proportional to even powers of f_{NL} , so the sign of the f_{NL} does not change the tensor two-point function. However, since the probability distribution function of the curvature fluctuations gets skewed, the PBH production efficiency increases (decreases) for $f_{NL} > 0$ ($f_{NL} < 0$). Therefore with $f_{NL} > 0$, the same amount of PBH can be produced by smaller amplitude (variance) scalar fluctuations, which results in smaller amplitude induced GWs [23, 24].

D. Primordial Black Holes

When a mode with an amplitude larger than the collapse threshold re-enters the horizon, the energy content inside the horizon collapses to a PBH that have a mass of the order of the mass inside the horizon. Since the mass of the PBH is comparable to the horizon mass, the PBH mass can be related to the wavenumber of the mode as $M_{\text{PBH}} = 20 \gamma M_{\odot} (k/\text{pc}^{-1})^{-2}$ or to its frequency [22]

$$M_{\text{PBH}} = 50 \gamma M_{\odot} \left(\frac{10^{-9} \text{ Hz}}{f} \right)^2, \quad (10)$$

where γ indicates the portion of the horizon that becomes PBH (we assume $\gamma = 0.2$ throughout this work). For a given scale, the fraction of the universe that turns into a PBH can be expressed as

$$\beta(k) = \int_{\zeta_{\text{th}}}^{\infty} \mathcal{P}(\zeta_{\text{cg}}(k)) d\zeta_{\text{cg}}(k), \quad (11)$$

where \mathcal{P} is the probability distribution function (p.d.f) of the curvature fluctuations, ζ_{th} is the threshold value

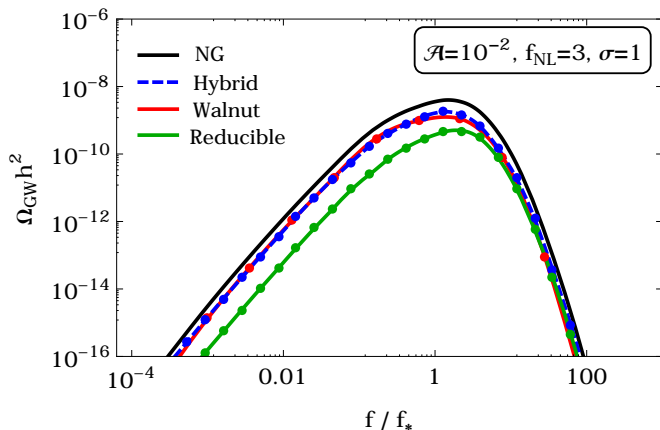


FIG. 8: Comparison of GW backgrounds from NG diagrams

$\mathcal{O}(0.1 - 1)$, and $\zeta_{\text{cg}}(k)$ is the coarse-grained density contrast : $\zeta_{\text{cg}}(k) = \int W(k)\zeta(k) d\ln k$, where W is a smoothing window function. Because PBHs are produced from the tail of the p.d.f of the curvature perturbations, the PBH amount is extremely sensitive to both threshold value and the details of the distribution function. Therefore, even small differences in either of them can lead to many orders of magnitude changes in PBH amount.

It is a remarkable possibility that PBHs can be whole or considerable fraction of DM [27–29]. The two mass ranges, $M \sim 10M_{\odot}$ and $M \sim 10^{-12}M_{\odot}$, are being discussed for such possibility [30–32]. It is even further interesting that the modes which produce the PBHs in these mass ranges lead to inevitable induced GW backgrounds. These backgrounds correspond to the frequency bands of nHz and mHz (see eq. (10)) which will be probed by PTA [33–35], SKA [36, 37] and LISA [38–40] experiments with enormous precision in close future [19, 22, 41]. However, whether PBHs are the dominant or completely negligible portion of the DM, induced GWs can reveal valuable information about the small scales.

III. RESULTS AND DISCUSSION

We obtain the spectrum of induced GWs by evaluating the two-point function given in eq. (5) at a moment when the corresponding mode is well inside the horizon (ie. $k\eta \gg 1$). The tensor modes are sourced around the horizon crossing, and GWs propagate freely afterwards. Since GWs are relativistic, their energy density scales like radiation, and one can obtain their current energy density using eq. (6).

In Figure 8, we show the contributions from Hybrid (dashed-blue), Walnut (solid-red) and Reducible (solid-green) diagrams together with total induced GW spectrum (solid-black) originating from non-Gaussian scalar sources (estimating $\Omega^{\text{Reduced}} + \Omega^{\text{Planar}} + \Omega^{\text{Non-Planar}} \simeq 2 \cdot \Omega^{\text{Reduced}}$ as indicated in the previous section.). The Walnut and Hybrid diagrams give almost same contribution to the GWs at every scale and the Reducible diagram is about an order of magnitude smaller.

In Figure 9, we show the stochastic GW background

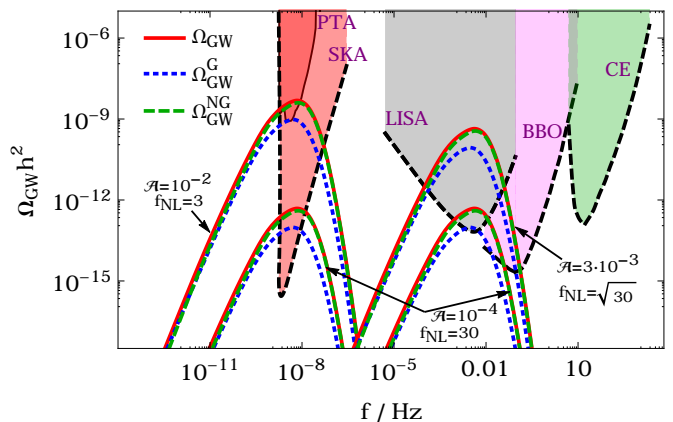


FIG. 9: $\Omega_{\text{GW}} h^2$ at distinct scales from G and NG Source

induced by Gaussian (dotted-blue) and non-Gaussian (dashed-green) scalar fluctuations together with the total induced GWs (solid-red) at nHz and mHz bands. We set $\sigma = 1$ for all curves. The labels Ω^{G} and Ω^{NG} , indicate the “source” of induced GWs (G or NG scalar fluctuations), but not the statistical properties of GWs because whether the source for GWs is Gaussian or not, the resultant GW background is non-Gaussian as it emerges from a cubic interaction [42–44] (see [45, 46] for a detailed discussion about the stochastic GWs). In all four cases, $\mathcal{A} f_{\text{NL}}^2 = 9 \cdot 10^{-2} \ll 1$ giving $P_{\zeta}^{\text{G}} > P_{\zeta}^{\text{NG}}$ all wavenumbers. However, although NG part of the scalar fluctuations are subdominant to G part, the GWs produced from NG scalar fluctuations are about an order of magnitude larger, $\Omega_{\text{GW}}^{\text{NG}} \simeq 9 \Omega_{\text{GW}}^{\text{G}}$.

For both LISA and PTA scales, there are two example GW signals, one has a large amplitude (bounded by the PBH bounds on scalar perturbations) and the other one small (near the sensitivity limit of the relevant GW experiment) showing that induced GWs are detectable for a wide range of scalar fluctuations (independent from the fact that PBHs are significant portion of the total energy density or not). The large amplitude GWs originates from scalar fluctuations leading to abundant amount of PBHs, which constitutes the totality or considerable fraction of the DM ¹ (ζ_{th} is set to 1.4). Notice that the scalar fluctuations producing PBH DM in the current universe have different amplitudes and β values for different (LISA and PTA) scales. This is because different mass PBHs form at different times, hence their energy density grows relative to the background energy density

¹ In the presence of positive non-Gaussianity parameter, β can be expressed as $\beta = \text{erfc}(Y_+(\zeta_{\text{th}})) + \text{erfc}(Y_-(\zeta_{\text{th}}))$, where $Y_{\pm}(\zeta) = \frac{1}{2\sqrt{2\mathcal{A}} f_{\text{NL}}} \left(-1 \pm \sqrt{1 + 4f_{\text{NL}}(\mathcal{A} + \zeta)} \right)$ [23]. The formation fraction, β , can be connected to the ratio of the energy density of PBH to DM in the current universe $\mathcal{F}(M) \equiv \frac{1}{\rho_{\text{DM}}} \frac{d\rho_{\text{PBH}}}{d\ln M} \simeq 6.7 \cdot 10^8 \gamma^{1/2} \beta(M) \sqrt{\frac{M_{\odot}}{M}}$ [30], where M_{\odot} is the solar mass.

different amount (as also seen in footnote 1). On the other hand, the small amplitude signal is chosen near the sensitivity limit of the both GW experiments to show the range of scalar fluctuations that can produce visible signal. Although we illustrate the GW signatures only at PTA-SKA and LISA scales, this study can be immediately extended for other GW experiments such as DECIGO/BBO [47] and Cosmic Explorer (CE) [48].

Since the NG scalar signal results from a convolution of G scalar signal (see eq. (9)), it is wider and its peak occurs at a wavenumber $\mathcal{O}(1)$ times larger than than G scalar signal (depending on the width) (see Figure 2). Also, induced GWs result from convolution of scalar sources, therefore the peak of the induced GWs is at a higher wavenumber than sourcing scalar functions. In result, the peak of the Reducible diagram has the highest wavenumber, the Hybrid and Walnut diagrams follow it and the Gaussian diagram has the lowest wavenumber peak. These results can be seen in Figures 8 and 9. Since the peak of NG scalar signal is at a higher wavenumber, even if the GWs sourced by G and NG sources have similar amplitude, the UV side is dominated by NG component in such a case. This difference in peaks might lead to observational consequences such as double peak (or change in the spectrum slope) if the separation between peaks are big enough for discrimination.

In the IR regime, ie. $k \ll k_*$, we have $k_* \sim p \sim |\mathbf{k} - \mathbf{p}| \gg k$ as the support of the momentum integrals are around wavenumber k_* , hence $F_T(u, u) \simeq \frac{27}{u^2} \sin^2(u/\sqrt{3})$ where $u \equiv p/k \gg 1$. In result, $P_{h_i} \propto k^3 \int \frac{F_T^2}{k^4} d(k\eta') (k\eta'') d(k\eta''') \propto k^3$. Therefore, in the IR regime, induced GWs scale with (nearly) the third power of the wavenumber independent of the fact that they are sourced by G or NG fluctuations.

It is also possible that the stochastic GW background is detected but, none of those signatures are observed, then this translates into stringent bounds on the NG parameter depending on the amplitude and (almost negligibly) the width of the GW background (observe the degeneracy in \mathcal{A} and f_{NL}). For this purpose, we calculated the induced GWs for different width parameters of the scalar signal, $\sigma = \{0.1, 0.25, 0.5, 1\}$, and found that the constraint for the non-detection of non-Gaussianity reads as $\mathcal{A} \cdot f_{\text{NL}}^2 \ll 10^{-2}$.

IV. CONCLUSIONS

Even though CMB and LSS (also potentially CMB distortion measurements) convey high quality and quantity data about the largest scales of the observable universe, the smaller scales are still vastly unexplored. In this work, we showed that small scales can be probed by GWs. Specifically, we show that subdominant or mildly non-Gaussian density fluctuations can produce more GWs than the Gaussian ones. Moreover, in the presence of local non-Gaussianity, GWs sourced by NG scalar fluctuations have a peak at a larger frequency than the GWs sourced by G fluctuations which might result in distinctive observational signatures.

GW energy density is proportional to the even powers of the non-Gaussianity parameter. For negative f_{NL} , one can have large amplitude scalar fluctuations and induced GWs without violating PBH bounds. More interestingly, for positive f_{NL} , these large amplitude scalar fluctuations produce abundant PBHs which can constitute the whole or some fraction of DM in the ranges $M \sim 10M_\odot$ and $M \sim 10^{-12}M_\odot$. The accompanying induced GW signals occur at nHz and mHz bands which will be probed by LISA and PTA with great precision. However, as we show that independent from the fact that PBHs are DM or completely negligible portion of current energy density, the statistical properties of the small scales can be imprinted on the induced GWs in a detectable way.

If the stochastic GW background induced by scalar fluctuations is detected, but not the signatures of the primordial non-Gaussianity in curvature fluctuations, this constrains f_{NL} parameter as follows $\mathcal{A} \cdot f_{\text{NL}}^2 \ll 0.01$.

Acknowledgments

It is a pleasure to thank Nicola Bartolo, Marco Peloso, Ignacy Sawicki, Lorenzo Sorbo, Bayram Tekin, Vincent Vennin and Alex Vikman for their critical reading of the draft, their feedback and useful discussions. We also thank Sohyun Park, Lorenzo Reverberi and Tom Zlosnik for illuminating discussions. Part of this research project was conducted using FZU computational resources and we acknowledge the help of Josef Dvoracek in this process. This work is supported by European Structural and Investment Funds and the Czech Ministry of Education, Youth and Sports (Project CoGraDS - CZ.02.1.01/0.0/0.0/15_003/0000437).

Note Added

As this work is being completed, Ref. [49] appeared which also studies the effects of NG scalar fluctuations on GW spectrum. However, their investigation focuses on the large f_{NL} limit, χ^2 distribution, hence their scalar fluctuations are dominantly Non-Gaussian and different than this study. Also Ref. [49] calculates the GW spectrum using only the first diagram given in Figure 7, neglecting the other two diagrams, which does not give the precise result, but gets the correct order of magnitude.

We note that the large f_{NL} limit, or χ^2 distribution, had been already studied in Ref. [22] which included all three diagrams in Figure 7.

- [1] P. A. R. Ade *et al.* [Planck Collaboration], *Astron. Astrophys.* **594**, A20 (2016) doi:10.1051/0004-6361/201525898 [arXiv:1502.02114 [astro-ph.CO]].
- [2] Y. Akrami *et al.* [Planck Collaboration], arXiv:1807.06211 [astro-ph.CO].
- [3] K. S. Dawson *et al.*, *Astron. J.* **151**, 44 (2016) doi:10.3847/0004-6256/151/2/44 [arXiv:1508.04473 [astro-ph.CO]].
- [4] D. J. Fixsen, E. S. Cheng, J. M. Gales, J. C. Mather, R. A. Shafer and E. L. Wright, *Astrophys. J.* **473**, 576 (1996) doi:10.1086/178173 [astro-ph/9605054].
- [5] A. Kogut *et al.*, *JCAP* **1107**, 025 (2011) doi:10.1088/1475-7516/2011/07/025 [arXiv:1105.2044 [astro-ph.CO]].
- [6] P. Andre *et al.* [PRISM Collaboration], *JCAP* **1402**, 006 (2014) doi:10.1088/1475-7516/2014/02/006 [arXiv:1310.1554 [astro-ph.CO]].
- [7] S. Mollerach, D. Harari and S. Matarrese, *Phys. Rev. D* **69**, 063002 (2004) [astro-ph/0310711].
- [8] K. N. Ananda, C. Clarkson and D. Wands, *Phys. Rev. D* **75**, 123518 (2007) [gr-qc/0612013].
- [9] D. Baumann, P. J. Steinhardt, K. Takahashi and K. Ichiki, *Phys. Rev. D* **76**, 084019 (2007) [hep-th/0703290].
- [10] M. H. Namjoo, H. Firouzjahi and M. Sasaki, *EPL* **101**, no. 3, 39001 (2013) doi:10.1209/0295-5075/101/39001 [arXiv:1210.3692 [astro-ph.CO]].
- [11] X. Chen, H. Firouzjahi, M. H. Namjoo and M. Sasaki, *EPL* **102**, no. 5, 59001 (2013) doi:10.1209/0295-5075/102/59001 [arXiv:1301.5699 [hep-th]].
- [12] J. Garcia-Bellido and E. Ruiz Morales, *Phys. Dark Univ.* **18**, 47 (2017) doi:10.1016/j.dark.2017.09.007 [arXiv:1702.03901 [astro-ph.CO]].
- [13] C. Pattison, V. Vennin, H. Assadullahi and D. Wands, *JCAP* **1710**, no. 10, 046 (2017) doi:10.1088/1475-7516/2017/10/046 [arXiv:1707.00537 [hep-th]].
- [14] G. Franciolini, A. Kehagias, S. Matarrese and A. Riotto, *JCAP* **1803**, no. 03, 016 (2018) doi:10.1088/1475-7516/2018/03/016 [arXiv:1801.09415 [astro-ph.CO]].
- [15] M. Biagetti, G. Franciolini, A. Kehagias and A. Riotto, *JCAP* **1807**, no. 07, 032 (2018) doi:10.1088/1475-7516/2018/07/032 [arXiv:1804.07124 [astro-ph.CO]].
- [16] J. M. Ezquiaga and J. Garcia-Bellido, *JCAP* **1808**, 018 (2018) doi:10.1088/1475-7516/2018/08/018 [arXiv:1805.06731 [astro-ph.CO]].
- [17] M. M. Anber and L. Sorbo, *Phys. Rev. D* **81**, 043534 (2010) doi:10.1103/PhysRevD.81.043534 [arXiv:0908.4089 [hep-th]].
- [18] E. Bugaev and P. Klimai, *Phys. Rev. D* **90**, no. 10, 103501 (2014) doi:10.1103/PhysRevD.90.103501 [arXiv:1312.7435 [astro-ph.CO]].
- [19] J. García-Bellido, M. Peloso and C. Unal, *JCAP* **1612**, no. 12, 031 (2016) [arXiv:1610.03763 [astro-ph.CO]].
- [20] R. Saito and J. Yokoyama, *Phys. Rev. Lett.* **102**, 161101 (2009) Erratum: [*Phys. Rev. Lett.* **107**, 069901 (2011)] doi:10.1103/PhysRevLett.102.161101, 10.1103/PhysRevLett.107.069901 [arXiv:0812.4339 [astro-ph]].
- [21] E. Bugaev and P. Klimai, *Phys. Rev. D* **83**, 083521 (2011) doi:10.1103/PhysRevD.83.083521 [arXiv:1012.4697 [astro-ph.CO]].
- [22] J. Garcia-Bellido, M. Peloso and C. Unal, *JCAP* **1709**, no. 09, 013 (2017) doi:10.1088/1475-7516/2017/09/013 [arXiv:1707.02441 [astro-ph.CO]].
- [23] C. T. Byrnes, E. J. Copeland and A. M. Green, *Phys. Rev. D* **86**, 043512 (2012) [arXiv:1206.4188 [astro-ph.CO]].
- [24] S. Young and C. T. Byrnes, *JCAP* **1308**, 052 (2013) doi:10.1088/1475-7516/2013/08/052 [arXiv:1307.4995 [astro-ph.CO]].
- [25] D. H. Lyth, *JCAP* **1205**, 022 (2012) [arXiv:1201.4312 [astro-ph.CO]].
- [26] T. Nakama, J. Silk and M. Kamionkowski, *Phys. Rev. D* **95**, no. 4, 043511 (2017) [arXiv:1612.06264 [astro-ph.CO]].
- [27] S. Bird, I. Cholis, J. B. Munoz, Y. Ali-Haïmoud, M. Kamionkowski, E. D. Kovetz, A. Raccanelli and A. G. Riess, *Phys. Rev. Lett.* **116**, no. 20, 201301 (2016) [arXiv:1603.00464 [astro-ph.CO]].
- [28] S. Clesse and J. Garcia-Bellido, *Phys. Dark Univ.* **15**, 142 (2017) doi:10.1016/j.dark.2016.10.002 [arXiv:1603.05234 [astro-ph.CO]].
- [29] M. Sasaki, T. Suyama, T. Tanaka and S. Yokoyama, *Phys. Rev. Lett.* **117**, no. 6, 061101 (2016) Erratum: [*Phys. Rev. Lett.* **121**, no. 5, 059901 (2018)] doi:10.1103/PhysRevLett.121.059901, 10.1103/PhysRevLett.117.061101 [arXiv:1603.08338 [astro-ph.CO]].
- [30] B. Carr, F. Kuhnel and M. Sandstad, *Phys. Rev. D* **94**, no. 8, 083504 (2016) [arXiv:1607.06077 [astro-ph.CO]].
- [31] M. Zumalacarregui and U. Seljak, *Phys. Rev. Lett.* **121**, no. 14, 141101 (2018) doi:10.1103/PhysRevLett.121.141101 [arXiv:1712.02240 [astro-ph.CO]].
- [32] J. Garcia-Bellido, S. Clesse and P. Fleury, *Phys. Dark Univ.* **20**, 95 (2018) doi:10.1016/j.dark.2018.04.005 [arXiv:1712.06574 [astro-ph.CO]].
- [33] Z. Arzoumanian *et al.* [NANOGrav Collaboration], *Astrophys. J.* **821**, no. 1, 13 (2016) [arXiv:1508.03024 [astro-ph.GA]].
- [34] L. Lentati *et al.*, *Mon. Not. Roy. Astron. Soc.* **453**, no. 3, 2576 (2015) [arXiv:1504.03692 [astro-ph.CO]].
- [35] R. M. Shannon *et al.*, *Science* **349**, no. 6255, 1522 (2015) [arXiv:1509.07320 [astro-ph.CO]].
- [36] C. J. Moore, R. H. Cole and C. P. L. Berry, *Class. Quant. Grav.* **32**, no. 1, 015014 (2015) [arXiv:1408.0740 [gr-qc]].
- [37] W. Zhao, Y. Zhang, X. P. You and Z. H. Zhu, *Phys. Rev. D* **87**, no. 12, 124012 (2013) [arXiv:1303.6718 [astro-ph.CO]].
- [38] P. Amaro-Seoane *et al.*, *GW Notes* **6**, 4 (2013) [arXiv:1201.3621 [astro-ph.CO]].
- [39] N. Bartolo *et al.*, *JCAP* **1612**, no. 12, 026 (2016) [arXiv:1610.06481 [astro-ph.CO]].
- [40] H. Audley *et al.* [LISA Collaboration], arXiv:1702.00786 [astro-ph.IM].
- [41] K. Inomata, M. Kawasaki, K. Mukaida, Y. Tada and T. T. Yanagida, *Phys. Rev. D* **95**, no. 12, 123510 (2017) doi:10.1103/PhysRevD.95.123510 [arXiv:1611.06130 [astro-ph.CO]].
- [42] J. R. Espinosa, D. Racco and A. Riotto, *JCAP* **1809**, no. 09, 012 (2018) doi:10.1088/1475-7516/2018/09/012 [arXiv:1804.07732 [hep-ph]].
- [43] N. Bartolo, V. De Luca, G. Franciolini, M. Peloso and A. Riotto, arXiv:1810.12218 [astro-ph.CO].

- [44] N. Bartolo, V. De Luca, G. Franciolini, M. Peloso, D. Racco and A. Riotto, arXiv:1810.12224 [astro-ph.CO].
- [45] C. Caprini and D. G. Figueroa, *Class. Quant. Grav.* **35**, no. 16, 163001 (2018) doi:10.1088/1361-6382/aac608 [arXiv:1801.04268 [astro-ph.CO]].
- [46] N. Bartolo *et al.*, arXiv:1806.02819 [astro-ph.CO].
- [47] K. Yagi and N. Seto, *Phys. Rev. D* **83**, 044011 (2011) Erratum: [*Phys. Rev. D* **95**, no. 10, 109901 (2017)] doi:10.1103/PhysRevD.95.109901, 10.1103/PhysRevD.83.044011 [arXiv:1101.3940 [astro-ph.CO]].
- [48] B. P. Abbott *et al.* [LIGO Scientific Collaboration], *Class. Quant. Grav.* **34**, no. 4, 044001 (2017) doi:10.1088/1361-6382/aa51f4 [arXiv:1607.08697 [astro-ph.IM]].
- [49] R. g. Cai, S. Pi and M. Sasaki, arXiv:1810.11000 [astro-ph.CO].